

Supplement of Biogeosciences, 12, 1993–2001, 2015
<http://www.biogeosciences.net/12/1993/2015/>
doi:10.5194/bg-12-1993-2015-supplement
© Author(s) 2015. CC Attribution 3.0 License.



Supplement of

Biostratigraphic evidence for dramatic Holocene uplift of Robinson Crusoe Island, Juan Fernández Ridge, SE Pacific Ocean

P. Sepúlveda et al.

Correspondence to: L. E. Lara (luis.lara@sernageomin.cl)

1 **Biostratigraphic evidence for dramatic Holocene uplift of**
2 **Robinson Crusoe Island, Juan Fernández Ridge, SE**
3 **Pacific Ocean**

4
5 **P. Sepúlveda¹, J. P. Le Roux^{1,2}, L.E. Lara^{3*}, G. Orozco^{3,2,1}, V. Astudillo¹**

6 [1]{Departamento de Geología, FCFM, Universidad de Chile}

7 [2]{Centro de Excelencia en Geotermia de los Andes, Santiago, Chile}

8 [3]{Volcano Hazards Program, Servicio Nacional de Geología y Minería, Santiago, Chile}

9 Correspondance to: Luis E. Lara (luis.lara@sernageomin.cl)

10
11 **Abstract**

12 A study of the biostratigraphy and sedimentology of Holocene deposits on Robinson
13 Crusoe Island (RCI) on the Juan Fernández Ridge (JFR) indicates that a dramatic but
14 localized uplift occurred since 8,000 BP, at a rate of about 8.5 mm/yr. In fact, supratidal
15 flats and sand layers with marine gastropods (mostly *Nerita* sp.) are now exposed *ca.* 70 m
16 a.s.l., and covered by transitional dunes. The last volcanic activity on RCI occurred at *ca.*
17 0.8 Ma (active hotspot located 280 km further west) and there is no sign of a compensating
18 bulge that explains this uplift, isobaths of the sea floor instead suggesting general
19 subsidence. However, modeling indicates that large-scale landslides followed by isostatic
20 rebound are a viable explanation, partially reflected in the low-resolution bathymetry of the
21 area.

22
23 **1 Introduction**

24 The Juan Fernández Ridge (JFR), located on the Nazca Plate in the Pacific Ocean off
25 central Chile (Fig. 1), is an 800 km long seamount and volcanic island chain extending E-
26 W at latitude 33°S. It has been interpreted as the expression of a fixed hotspot (Von Heune

27 *et al.*, 1997; Montelli *et al.*, 2006) related to a primary mantle plume in the sense of
28 Courtillot *et al.* (2003) or as part of a ‘hot line’ (Bonatti *et al.*, 1977). According to the
29 plume hypothesis, active diapiric plumes arising from the core-mantle boundary form
30 submarine volcanic *plateaux* or island chains within oceanic plates. As the plate moves
31 away due to sea-floor spreading, these volcanoes are extinguished and new volcanic
32 edifices arise over the active hotspot, forming age progressive island chains such as the
33 Hawaiian-Emperor seamount chain. The plume hypothesis has been challenged, however,
34 because some of its predictions have not been confirmed by observation, and plate tectonic
35 processes are thought to be playing a role (*e.g.*, Foulger, 2010).

36 A remarkable feature of hotspot ocean islands is their complex history of vertical
37 displacement (*e.g.*, Ramalho *et al.*, 2013). Uplift and subsidence, as earlier noted by
38 Charles Darwin in the 19th century, respond to a number of large-scale processes better
39 known at present as the growth of the underlying swell and the related isostatic rebound,
40 bulging effects resulting from loading of nearby islands and seamounts (*e.g.*, Bianco *et al.*,
41 2005), changes of density in the mantle, intrusions at the base of the edifice (*e.g.*, Klügel *et*
42 *al.*, 2005) and gradual cooling of the lithosphere. However, giant landslides can also trigger
43 sudden uplift as inferred for archetypical hotspot volcanoes such as Hawaii (*e.g.*, Smith and
44 Wessel, 2000).

45 Although most of the active oceanic islands are subsiding (as the Surtsey island in the last
46 decades; *e.g.*, Moore *et al.*, 1992), here we present evidence for a very high Holocene uplift
47 rate of Robinson Crusoe Island (RCI) and discuss a possible mechanism together with
48 implications for the long-term evolution of this ocean island.

49 **2 Geological and geomorphological background**

50 The JFR is an island-seamount chain largely formed by the Miocene (*ca.* 9 Ma) O’Higgins
51 guyot and seamount (Von Heune *et al.*, 1997), with lavas dating back to *ca.* 4 Ma on RCI
52 and nearby Santa Clara Island (Fig. 1), and *ca.* 1 Ma on Alejandro Selkirk Island about 120
53 km away (Farley *et al.*, 1993). The relief on the western, arid part of RCI is characterized
54 by coastal cliffs bordering a terrace at about 70 m a.s.l., which is especially well developed
55 in the southwestern panhandle (Fig. 1). This terrace is formed on top of a post-shield

Comentario [LLP1]: Paragraph changed according to reviewer suggestions in order to mention other well-known processes after Darwin

Comentario [LLP2]: Mention to Surtsey as suggested

56 volcanic platform of middle Pleistocene age from which pyroclastic cones emerge, reaching
57 a maximum elevation of 915 m (Lara *et al.*, 2013). Holocene sedimentary deposits are
58 restricted to the terrace in the vicinity of Tierra Blanca Bay. The latter name is applied (in
59 Spanish) to a succession described by Morales (1987) as poorly consolidated, calcareous
60 sandstones at the base grading upward into tuffaceous sandstones with numerous fossils. In
61 the transition zone are *Acanthina* and *Lima* fossils with bryozoa fragments, whereas the
62 tuffaceous sandstones host *Luccinea*, *Distoechia*, *Bythinia*, *Orcula*, *Tropicorbis*, *Ena*, and
63 *Cyrena spp.* indicating a Pleistocene-Holocene age, based on a similar fossil assemblage on
64 the continent at this latitude (Covacevich, 1971; Valenzuela, 1978). The Bahía Tierra
65 Blanca Formation has its base at a variable elevation but generally at *ca.* 70 m above the
66 present mean sea level, where active, incipient barchan dunes (Morales, 1987), partially
67 rework the succession described above.

68 **3 Material and Methods**

69 Field campaigns were carried out on RCI in 2011-2013, during which geological mapping
70 was undertaken, stratigraphic sections were measured, and samples were collected for
71 further analysis. Laboratory work consisted of fossil identification, petrographic
72 microscopy, sieve and Mastersizer 2000 (Malvern Instruments, Malvern, United Kingdom)
73 analysis of the sediment grain-size distribution, and radiocarbon dating (Beta Analytic Inc.,
74 Miami, Accelerator Mass Spectrometer) of gastropods. The latter were collected mostly
75 from sites 1 and 5 (Fig.1). Several specimens were hand-picked from bulk samples and
76 three were selected for dating based on their stratigraphic position and systematics. AMS
77 radiocarbon dates were first corrected for the global marine reservoir effect (*e.g.*, Ulm,
78 2006) with the Marine IntCal09 calibration program (Reimer *et al.*, 2009). For the localized
79 reservoir correction a Delta-R value of 373 ± 76 from a site nearby
80 (<http://radiocarbon.pa.qub.ac.uk/marine/>) was used. Elevations were measured with a dGPS
81 Trimble®NetRS® and barometric altimeters with respect to the current sea-level and
82 corrected for the regional sea level and daily variation
83 (<http://www.shoa.cl/mareas/tablademarea.html>) with a nominal uncertainty of 5 m.

84 **4 Depositional environments**

85 Four lithostratigraphic units and three lithofacies were identified in the Bahía Tierra Blanca
86 Formation, which reaches a total thickness between 2 and 4 m at any specific locality (Fig.
87 2).

88 Unit 1 is largely composed of facies 1, which discordantly overlies weathered, basaltic
89 lavas. It consists of very poorly consolidated, slightly calcareous, reddish brown to reddish
90 purple deposits ranging in size from very fine sandstone to claystone. Their composition is
91 made up of volcanic ash mixed with the underlying, weathered lava material. These
92 deposits contain up to 2% bioclasts (mostly marine bivalves) together with pellets. The
93 most striking feature of this facies is ubiquitous, up to 1 m diameter teepee structures,
94 which display prominent edges elevated 3-5 cm above the central parts (Fig. 2). The cracks
95 have been filled in by sands from the overlying unit. Locally, shallow channels and rill
96 marks are present.

97 While the reddish to purplish brown color suggests a mainly subaerial environment, the
98 presence of teepee structures with elevated rims indicate frequent flooding and drying
99 cycles. These, as well as the occurrence of pellets, are typical of supratidal flats (*e.g.*,
100 Assereto and Kendall, 1977), which concurs with the presence of shallow channels
101 probably reflecting tidal creeks. The general scarcity of hard-shell fossils in this facies can
102 be interpreted as representing a generally hostile environment subjected to frequent dry
103 periods between spring high tides, followed by seawater flooding that would kill land-
104 dwelling snails and other organisms. Marine shells washed in during spring high tides
105 would probably accumulate along the shoreline. Soft-bodied forms more tolerant to such
106 conditions, on the other hand, would not be preserved in such an oxidizing environment.

107 Facies 2 is present in units 2 and 3, which differ mainly in the darker brown color of the
108 latter due to a thin brownish film coating the grains. Both units 2 and 3 show large-scale,
109 low angle planar cross-bedding and horizontal lamination, but in unit 3, high-angle planar
110 and trough cross-bedding are locally present (SM, Fig. A). The 1-2 cm thick cross-beds are
111 formed by alternating light and darker-colored grains without any evident gradation.
112 Rhizcretions are present in the uppermost parts of both units, where individual forms may
113 reach 1.5 m in length (Fig. 3). Although rhizcretions and vertebrate burrows are generally
114 rare, some parts have a fairly high density of the former. Unit 2 is capped locally by whitish

115 calcrete indicating incipient pedogenesis. Gastropods such as *Succinea*, *Fernandezia*, and
116 *Nerita* occur in the middle to upper part of unit 2. Petrographically, the sandstone is well
117 sorted with subrounded grains, lacking a matrix, and cement being only locally present.
118 Bioclasts compose around 55% of the rock, including brachiopod and pelecypod fragments,
119 echinoderm spines, bryozoa, red algae, foraminifers, and sub-rounded pellets. The rest of
120 the composition is made up of volcanic fragments and minerals such as K-feldspar,
121 plagioclase, clinopyroxene, and olivine, with rare quartz. Grain-size analysis of several
122 samples from this facies shows a small traction load, a prominent and very well-sorted
123 saltation load, and a medium- to well-sorted suspension load (SM, Fig. B). This facies is
124 interpreted as reflecting coastal eolian deposits perhaps locally affected by weak wave
125 action. This is supported by the reddish brown color of the sandstones, their predominantly
126 fine grain-size with cumulative curves typical of wind-blown deposits, and the presence of
127 the land-dwelling snails *Succinea* and *Fernandezia*, as well as root and burrow systems.
128 The horizontally laminated strata probably formed in sand sheets between low dunes,
129 which might have been parabolic in shape as suggested by the dominance of low-angle
130 planar cross-bedding. Some were subsequently converted into *dikaka* dunes by vegetation.
131 Some low-angle cross-bedding might represent reworking by dissipated wave action during
132 storms and spring high tides along the landward edges of wide supratidal flats. This could
133 also explain the presence of thick-shelled *Nerita* (a marine species) in Unit 2. The presence
134 of fragmented marine invertebrates indicates a marine source for most of these sands,
135 which suggests that they formed at a low elevation above sea level.

136 Facies 3 is composed of greyish white, medium sorted sandstones interbedded with gravel.
137 The sandstones consist of bioclasts (45-57%) mostly represented by marine shell fragments
138 including bivalves, gastropods such as *Succinea*, bryozoa, algae, and foraminifers, together
139 with lithic volcanic fragments (27-45%) and volcanic minerals such as pyroxene, olivine,
140 and felsic minerals (10-17%). The gravels are greyish brown and matrix- to clast-
141 supported, with the clasts reaching up to 5 cm in diameter. They are mainly volcanic and
142 angular. Locally, calcretes are present at the top of this facies. This facies clearly represents
143 fluvial deposits, probably consisting of shallow, quick-flowing ephemeral streams with
144 gravelly channels and sandy bars. These most likely drained exposed basalts on the fringes
145 of the eolian sand sheets, but also reworked the latter to incorporate the marine bioclasts.

146

147 **5 Radiocarbon dating**

148 Specimens of *Nerita* (SOM, Fig. C) from the eolian sandstones of unit 2 yielded calibrated
149 radiocarbon ages between 8,320 and 8,030 BP (conventional radiometric age of 7,860±40
150 years BP). Values corrected for the global marine reservoir effect (with a local Delta-R of
151 373±76 as obtained for the similar entry at <http://radiocarbon.pa.qub.ac.uk/marine/>
152 correspond to 7,550±90 years BP (see Table 1). These marine species were probably
153 reworked from the supratidal flats of unit 1 and would thus represent the age of the latter.
154 On the other hand, land-dwelling species as *Succinea* and *Fernandezia* (e.g., Odhner, 1922)
155 from units 3 and 4 gave calibrated radiocarbon ages between 5,440 and 5,090 years BP
156 (4,580±30 conventional years BP) and 7,680 and 7,580 years BP (6,790±40 conventional
157 years BP), respectively.

158 **6 Discussion**

159 The stratigraphic succession of the Bahía Tierra Blanca Formation suggests that supratidal
160 conditions existed in the southwestern panhandle of RCI between 8,320 and 8,030 years BP
161 (horizons with *Nerita*). It is unlikely that the tides reached more than 1-2 m above the mean
162 sea level, because topographic tide-enhancing conditions such as funnel-shaped estuaries
163 could not have existed due to the absence of large rivers on this part of the island. These
164 supratidal flats were encroached upon by eolian coastal plain deposits at around 5,430 years
165 BP (horizons with *Succinea* and *Fernandezia*) and finally fluvial sedimentation as the sea-
166 level receded further during the late Holocene Climatic Optimum (Davis *et al.*, 2003;
167 Koshkarova and Koshkarov, 2004), when the southwestern panhandle would have received
168 more rain. The present elevation of the supratidal deposits on a marine terrace at 70 m a.s.l.
169 indicates a very rapid relative sea-level fall since that time. Furthermore, it can be assumed
170 that the eolian deposits of units 2 and 3 were also not more than a few meters above the
171 tidal flats, as they had apparently been reworked locally by waves. This is supported by the
172 low-angle cross-bedding typical of beaches and the presence of reworked *Nerita*. The latter
173 could not have been blown uphill by wind, considering that they reach up to 1 cm in

174 diameter (Appendix A). Assuming that they were not more than 2 m above the tidal flats or
175 beaches, a relative sea-level fall at least 8.5 mm/year is implied.

176 Eustatic sea-levels have been well below the present-day level over the last 20,000 years
177 (Bindoff *et al.*, 2007; Fleming *et al.*, 1998). In Tahiti and almost all other regions of the
178 world where detailed records exist (*e.g.*, Lambeck *et al.*, 2002), there are indications that
179 the sea-level at 8,000 years BP was about 15 m below that of the present (Fleming *et al.*,
180 1998; Milne *et al.*, 2005). This rules out an eustatic highstand at the time. A mean uplift
181 rate of around 8.5 mm/yr is extremely high, considering that the average rate of uplift of the
182 Andes has been only about 0.2-0.3 mm/yr since the Late Miocene (Gregory-Wodzicki,
183 2000) and uplift rates of other ocean islands were < 0.33 mm/yr (*e.g.*, in the oldest
184 Hawaiian islands as reported by McMurtry *et al.*, 2004 and references therein). Ocean
185 islands with evidence of significant freeboard (*e.g.* Cape Verde) show uplift rates <0.4
186 mm/yr (Ramalho *et al.*, 2010a; 2010b). This high vertical displacement rate is only
187 comparable with the subsidence rate of the active Hawaii Island, which sinks at *ca.* 2.6
188 mm/yr (McMurtry *et al.*, 2004). No further evidence of such an uplift is recorded at RCI,
189 which in turn suggests a very localized process.

190 The dramatic Holocene uplift of RCI cannot be explained as a flexural response to the
191 loading exerted by the edifices created by the active hotspot. Isobaths (after Becker *et al.*,
192 2009; see also Rodrigo and Lara, 2014) show that the sea floor north of the JFR descends
193 from 3,800 m northwest of Alejandro Selkirk to about 4,000 m north of the latter, from
194 where it declines further to reach 4,200 m north of RCI and 4,300 m northeast thereof.

195 **There is thus no direct evidence for the existence of a bulge upon which RCI would be**
196 **situated. The bathymetry in fact shows a negative anomaly for this part of the oceanic crust.**

197 General subsidence could occur in the wake of a mantle plume migrating away from a
198 particular area, as this part of the lithosphere would no longer be sustained by it, combined
199 with the load exerted by the shield volcano. The generation of new islands and seamounts
200 above a fixed mantle plume could cause loading and subsidence of the crust accompanied
201 by the formation of an adjacent, compensating bulge, and hence local uplift. **A theoretical**
202 **bulge caused by the youngest volcanism at Friday/Domingo seamounts (250 km further**
203 **west of RCI) is not enough to explain uplift at RCI if realistic values for elastic parameters**

Comentario [LLP3]: Paragraph slightly modified according to suggestions

204 are considered (*e.g.*, Manríquez *et al.*, 2013). Watts and Ten Brink (1989), *e.g.*, proposed
205 the existence of such a bulge 300 km from the present hotspot on Hawaii Island, which
206 formed in response to subsidence of 1,300 m at the latter locality over the last 500,000
207 years (McMurtry *et al.*, 2010). Evidence of >20 m uplift is found at Oahu in the now
208 emerged coral reefs (McMurtry *et al.*, 2010). However, there is no evidence of recent
209 Holocene volcanism further west at a distance short enough to promote uplift at RCI. In
210 addition, 3D modeling of the lithospheric flexure seaward of the trench (Manríquez *et al.*,
211 2013) shows that even more complex loads (seamount loading, bending of the lithosphere
212 near the trench and sedimentary fill inside the trench south of 34°S) do not generate a
213 flexural response beyond 350 km from the outer rise.

Comentario [LLP4]: Paragraph added to explain why a bulge, if any, should cause a short-wave anomaly not enough to cause uplift at RCI

214 Intrusion at the base of the edifice, as proposed for Canary Islands (Klügel *et al.*, 2005) and
215 Cape Verde (Madeira *et al.*, 2010; Ramalho *et al.*, 2010b) cannot be ruled out. However,
216 because of the absence of volcanism younger than *ca.* 1 Ma and the rapid displacement of
217 the Nazca Plate we have a reasonable doubt about the occurrence of this process in the
218 Holocene.

Comentario [LLP5]: Intrusion at the base of the edifice, which cannot be ruled out, is commented and discussed as a theoretical possibility, which we don't favor because of geological evidence

219 Another possibility could be the development of large-scale landslides. The southwestern
220 part of the island is characterized by steep coastal cliffs, and the area lies opposite Santa
221 Clara Island that is thought to have originally formed part of a larger island incorporating
222 RCI (Danton, 2004). The two islands might have been separated during a large-scale
223 landslide event (or events), which in turn may have caused isostatic rebound. The latter is
224 thought to be larger on oceanic plates than on continental plates because of their more
225 limited thickness. In hotspot environments and other high heat-flow areas such as spreading
226 boundaries the asthenosphere should be less viscous, so that rebound rates may increase.
227 Similar events have been reported in Hawaii during the last 2 m.y. (McMurtry *et al.*, 2004).
228 Smith and Wessel (2000) calculated that the removal of 800 km³ of material during the
229 Alike landslide elevated the adjacent terrain by about 17 m, whereas McMurtry *et al.*
230 (2004) calculated uplift of 109 m for a volume of 5,000 km³ removed during the Nuuanu
231 landslide. Taking into account an elastic thickness of *ca.* 10 km (Manríquez *et al.*, 2013),
232 about 2,000 km³ of material (*ca.* 25% of the initial volume) would thus have had to be
233 removed to account for >70 m of uplift at RCI. Such a large mass wasting deposit is not

234 evident in the low resolution bathymetry around the RCI, but the caldera-like structure open
235 to the south and some rough relief on the distal flanks suggest that a landslide is a plausible
236 hypothesis.

237

238 **7 Conclusions**

239 Large-scale landslides around ocean islands can probably be attributed to an increase in
240 local slopes generated by the construction of volcanic edifices and the development of
241 rifting. At RCI there has been no major surface volcanic activity since about 3 Ma, with
242 only minor post-shield activity at 0.8 Ma (Lara *et al.*, 2013). Nevertheless, the topography
243 of RCI is even steeper than that of Hawaii, which could have allowed sliding to take place.
244 As modeled by Smith and Wessel (2000), directed giant landslides generate isostatic
245 rebound which is larger over the failed flank and spatially asymmetric. Apparent tilting of
246 the Pliocene volcanic pile could be another expression of this process.

247 Thus, biostratigraphic evidence of the exposure of former supratidal flats 70 m above the
248 present sea level, could be related to a large Holocene landslide not previously detected.
249 These findings highlight the importance of biological markers in order to better understand
250 the complex evolution of ocean islands.

251

252 **Appendix A: Calculation of required wind speed)**

253 All equations can be found in Le Roux (2005).

254 Shell density (calcite): $\rho_s = 2.85 \text{ g cm}^{-3}$.

255 Shell shape: Ellipsoid, long axis = 1 cm, intermediate axis = 0.75 cm, short axis = 0.35 cm.

256 Nominal diameter: $D_n = \sqrt[3]{(1)(0.75)(0.35)} = 0.64 \text{ cm}$

257 Water density: $\rho_w = 0.9982 \text{ g cm}^{-3}$.

258 Water dynamic viscosity: $\mu_w = 0.01 \text{ g cm}^{-1} \text{ s}^{-1}$.

259 Air density: $\rho_a = 0.0012 \text{ g cm}^{-3}$.

260 Submerged density of shell in water: $\rho_\gamma = \rho_s - \rho_w = 2.85 - 0.9982 = 1.8518 \text{ g cm}^{-3}$.

261 Acceleration due to gravity: $g = 981 \text{ cm s}^{-2}$.

262 Dimensionless grain size (water): $D_{ds} = D_n \sqrt[3]{\frac{\rho g \rho_\gamma}{\mu^2}} = 0.64 \sqrt[3]{\frac{(0.9982)(981)(1.8518)}{(0.01)^2}} = 168.14$.

263 Dimensionless settling velocity of nominal sphere in water:

264 $W_{ds} = \sqrt{2.531 D_{ds} + 160} = \sqrt{(2.531)(168.14) + 160} = 24.2$.

265 Real settling velocity of nominal sphere in water:

266 $W_s = \frac{W_{ds}}{\sqrt[3]{\rho^2 / \mu g \rho_\gamma}} = \frac{24.2}{\sqrt[3]{(0.9982)^2 / (0.01)(981)(1.8518)}} = 63.69 \text{ cm s}^{-1}$.

267 Real settling velocity of ellipsoid:

268 $W_e = -W_s \left\{ 0.572 \left[1 - \left(\frac{D_t}{D_l} \right) \right]^{2.5} - 1 \right\} = -63.69 \left\{ 0.572 \left[1 - \left(\frac{0.75}{1} \right) \right]^{2.5} - 1 \right\} = 62.55 \text{ cm s}^{-1}$

269 Dimensionless settling velocity of ellipsoid in water:

270 $W_{de} = W_e \sqrt[3]{\rho^2 / \mu g \rho_\gamma} = 62.55 \sqrt[3]{(0.9982)^2 / (0.01)(981)(1.8518)} = 23.76$

271 Dimensionless critical shear stress in air for $W_{de} > 11$, assuming that β_c levels off as in water:

272 $\beta_c = 0.00664 \log_{10} W_{de} + 0.00936 = (0.00664)(1.3758) + 0.00936 = 0.0185$

273

274 Critical shear velocity U_{*c} in air:

275 $U_{*c} = \sqrt{\frac{\beta_c g D \rho_\gamma}{\rho}} = \sqrt{\frac{(0.0185)(981)(0.64)(2.85 - 0.0012)}{0.0012}} = 166 \text{ cm s}^{-1}$.

276 Assuming a fully rough boundary, required wind speed measured 10 m above the ground:

277 $U_a = U_{*c} \left[2.5 \ln \left(\frac{y}{D} \right) + 8.5 \right] = 166 \left[2.5 \ln \left(\frac{1000}{0.64} \right) + 8.5 \right] = 4462.9 \text{ cm s}^{-1} \approx 160 \text{ km hr}^{-1}$.

278

279 **Acknowledgements**

280 This research was supported by Fondecyt 1110966 project granted to L.E. Lara and is also
281 part of a collaborative effort to better understand fundamental processes in the oceanic
282 islands of the Nazca Plate. J.P. Le Roux worked under the auspices of Project CONICYT-
283 FONDAF 15090013. J.C. Baez kindly provided dGPS equipment and data reduction. S.N.
284 Nielsen and S. Letelier advised on the fossil record. CONAF authorized scientific research
285 in this protected area and DIFROL provided logistical support during the last 2013 field
286 campaign. The referees's comments are greatly appreciated.

287 **References**

- 288 Assereto, R.L.A.M, and Kendall, C.G.St.C.: Nature, origin and classification of peritidal
289 tepee structures and related breccias, *Sedimentology*, 24, 153-210, 1977.
- 290 Bianco, T. A., Ito, G., Becker, J.M., and García, M.O.: Secondary Hawaiian volcanism
291 formed by flexural arch decompression, *Geochem. Geophys. Geosyst.* (6), Q08009,
292 doi:10.1029/2005GC000945, 2005.
- 293 Becker, J.J., Sandwell, D.T., Smith, W.H.F., Braud, J., Binder, B., Depner, J., and
294 Weatherall, P.: Global bathymetry and elevation data at 30 arc seconds resolution:
295 SRTM30_PLUS, *Mar Geod*, 32(4), 355-371, 2009.
- 296 Bindoff, N.L., J. Willebrand, V. Artale, A. Cazenave, J. Gregory, S. Gulev, K. Hanawa, C.
297 Le Quéré, S. Levitus, Y. Nojiri, C.K. Shum, L.D. Talley, and Unnikrishnan, A.:
298 Observations: Oceanic Climate Change and Sea Level, In: *Climate Change 2007: The*
299 *Physical Science Basis. Contribution of Working Group I to the Fourth Assessment*
300 *Report of the Intergovernmental Panel on Climate Change [Solomon, S., D. Qin, M.*
301 *Manning, Z. Chen, M. Marquis, K.B. Averyt, M. Tignor and H.L. Miller (eds.)].*
302 *Cambridge University Press, Cambridge, United Kingdom and New York, NY, USA,*
303 *2007.*
- 304 Bonatti, E., Harrison, C. G. A., Fisher, D. E., Honnorez, J., Schilling, J. G., Stipp, J. J., and
305 Zentilli, M.: Easter volcanic chain (southeast Pacific): A mantle hot line. *J. Geophys.*
306 *Res.*, 82(17), 2457-2478, 1977.
- 307 Courtillot, V., Davaille, A., Besses, J., and Stock, J.: Three distinct types of hotspots in the
308 Earth's mantle, *Earth Planet Sc Lett*, 205, 295-308, 2003.

309 Covacevich, V.: Los moluscos pleistocénicos y holocénicos de San Vicente de Tagua
310 Tagua, Memoria de Título (unpublished thesis), Universidad de Chile, Santiago, 1971.
311 Danton, P.H.: Plantas silvestres de la isla Robinson Crusoe: Guía de Reconocimiento.
312 Corporación Nacional Forestal, Región de Valparaíso, Viña del Mar, 2004.
313 Davis, B.A.S., Brewer, S., Stevenson, A.C., and Guiot, J.: The temperature of Europe
314 during the Holocene reconstructed from pollen data, *Quaternary Sci Rev*, 22(15–17),
315 1701-1716, 2003.
316 Farley, K. A., A. R. Basu, and Craig, H.: He, Sr and Nd isotopic variations in lavas from
317 the Juan Fernandez Archipelago, SE Pacific, *Contrib Mineral Petr*, 115 (1), 75-87, 1993.
318 Fleming, K., Johnston, P., Zwartz, D., Yokoyama, Y., Lambeck, K., and Chappell, J.:
319 Redefining the eustatic sea-level curve since the Last Glacial Maximum using far- and
320 intermediate-field sites, *Earth Planet Sc Lett*, 163, 327-342, 1998.
321 Foulger, G.R.: *Plates vs. Plumes: A Geological Controversy*, Wiley-Blackwell, New York,
322 364 p., 2010.
323 Gregory-Wodzicki, K.M.: Uplift history of the Central and Northern Andes: a review, *Geol*
324 *Soc Am Bull*, 112, 1091-1105, 2000.
325 Klügel, A., T. Hansteen, and K. Galipp. Magma storage and underplating beneath Cumbre
326 Vieja volcano, La Palma (Canary Islands). *Earth and Planetary Science Letters*, 236(1-
327 2):211–226, 2005.
328 Koshkarova, V.L., and Koshkarov, A.D.: Regional signatures of changing landscape and
329 climate of northern central Siberia in the Holocene, *Russ. Geol. Geophys.*, 45(6), 672-
330 685, 2004.
331 Lambeck, K., Yokoyama, Y., and Purcell, T.: Into and out of the Last Glacial Maximum:
332 sea-level change during Oxygen Isotope Stages 3 and 2. *Quaternary Science Reviews*,
333 21(1), 343-360, 2002.
334 Lara, L.E., Reyes, J., Piña-Gauthier, M. and Orozco, G.: Geological evidence of a post
335 shield stage at the Juan Fernandez Ridge, Nazca Plate, IAVCEI Scientific Assembly
336 Kagoshima, Abstracts, 2013.
337 Le Roux, J.P.: Grains in motion: A review, *Sedimentary Geology*, 178, 285-313, 2005.
338 Madeira, J., Mata, J., Mourão, C., Brum da Silveira, A., Martins, S., Ramalho, R.S., and D.
339 Hoffmann. Volcano-stratigraphic and structural evolution of Brava Island (Cape Verde)

340 from $^{40}\text{Ar}/^{39}\text{Ar}$, U/Th and field constraints. *Journal of Volcanology and Geothermal*
341 *Research*, 196(3-4):219–235, 2010.

342 Manríquez, P., Contreras-Reyes, E., and Osses, A., Lithospheric 3-D flexure modelling of
343 the oceanic plate seaward of the trench using variable elastic thickness, *Geophys J Int*,
344 ggt464, 2013.

345 McMurtry, G.M., Campbell, J.F., Fryer, G.J., Smith, J.R., and Fietzke, J.: Uplift of Oahu,
346 Hawaii, during the past 500 k.y. as recorded by elevated reef deposits, *Geology*, 38, 27-
347 30, 2010.

348 McMurtry, G.M., Watts, P., Fryer, G.J., Smith, J.R., and Imamura, F.: Giant landslides,
349 mega-tsunamis, and paleo-sea level in the Hawaiian Islands, *Mar Geol*, 203, 219-233,
350 2004.

351 Milne, G.A., Long, A.J., and Bassett, S.E.: Modelling Holocene relative sea-level
352 observations from the Caribbean and South America, *Quaternary Sci Rev*, 24(10-11),
353 1183-1202, 2005.

354 Morales, A.: Geología de las islas Robinson Crusoe y Santa Clara, Archipiélago de Juan
355 Fernández, V. Región, Chile: Memoria de Título (unpublished thesis), Universidad
356 Católica del Norte, Antofagasta, 1987.

357 Montelli, R., Nolet, G., Dahlen, F.A., and Masters, G.: A catalogue of deep mantle plumes:
358 New results from finite-frequency tomography, *Geochem Geophys Geosy*, 7(11), 2006.

359 Moore, J.G., S. Jakobsson, and J. Holmjàrn: Subsidence of Surtsey Volcano, 1967-1991,
360 *Bulletin of Volcanology* 55 (1-2), 1992.

361 Odhner, N.: Mollusca from Juan Fernández and Easter Island, Addenda, *in* Skottsberg, C.
362 (ed.), *The Natural History of Juan Fernández and Easter Island*: Almqvist and Wiksells,
363 Uppsala, 1922.

364 Ramalho, R.S., Quartau, R., Trenhaile, A.S., Mitchell, N.C., Woodroffe, C.D., and Ávila,
365 S.P.: Coastal evolution on volcanic oceanic islands: A complex interplay between
366 volcanism, erosion, sedimentation, sea-level change and biogenic production, *Earth- Sci*
367 *Rev*, 127, 140-170, 2013.

368 Ramalho, R.S., Helffrich, G., Cosca, M., Vance, D., Hoffmann, D. and Schmidt, D.N.:
369 Episodic swell growth inferred from variable uplift of the Cape Verde hotspot islands.
370 *Nature Geoscience*, 3(11):774–777, 2010a.

371 Ramalho, R.S., Helffrich, G., Schmidt, D.N., and Vance, D.: Tracers of uplift and
372 subsidence in the Cape Verde Archipelago. *Journal of the Geological Society*,
373 167(3):519–538, 2010b.

374 Reimer, P. J., Baillie, M. G. L., Bard, E., Bayliss, A., Beck, J. W., Blackwell, P. G., Bronk
375 Ramsey, C., Buck, C. E., Burr, G. S., Edwards, R. L., Friedrich, M., Grootes, P. M.,
376 Guilderson, T. P., Hajdas, I., Heaton, T. J., Hogg, A. G., Hughen, K. A., Kaiser, K. F.,
377 Kromer, B., McCormac, F. G., Manning, S. W., Reimer, R. W., Richards, D. A.,
378 Southon, J. R., Talamo, S., Turney, C. S. M., van der Plicht, J., and Weyhenmeyer, C.
379 E.: IntCal09 and Marine09 radiocarbon age calibration curves, 0-50,000 years cal BP,
380 *Radiocarbon*, 51(4), 1111-1150, 2009.

381 Rodrigo, C. and Lara, L.E.: Plate tectonics and the origin of the Juan Fernández Ridge:
382 analysis of bathymetry and magnetic patterns, *Lat. Am. J. Aquat. Res.* 42 (4), 2014.

383 Smith, J.R., and Wessel, P.: Isostatic consequences of giant landslides on the Hawaiian
384 Ridge, *Pure Appl Geophys*, 157, 1097-1114, 2000.

385 Ulm, S.: Australian marine reservoir effects: a guide to ΔR values, *Australian Archaeology*,
386 57-60, 2006.

387 Valenzuela, E.: Pleistoceno marino en la isla Robinson Crusoe, *Comunicaciones*, 22, 32-35,
388 1978.

389 Von Heune, R., Corvalán, J., Flueh, E.R., Hinz, K., Korstgard, J., Ranero, C.R., and
390 Weinrebe, W.: Tectonic control of the subducting Juan Fernández Ridge on the Andean
391 margin near Valparaíso, Chile, *Tectonics*, 16(3), 474-488, 1997.

392 Watts, A.B. and Ten Brink, S.: Crustal structure, flexure, and subsidence history of the
393 Hawaiian Islands: *J. Geophys. Res.* 94 (B8), 10,473-10,500, 1989.

394

395 Table 1. Radiocarbon dates for gastropods from RCI

Table 1. Radiocarbon dates for gastropods from Robinson Crusoe Island									
Site	Sample	Lab. Number	Conventional radiocarbon age (yBP)	C13/C12 ratio	Calibrated age (Cal yBP) 2 σ	Reservoir corrected age Delta-R= 313 \pm 76	Calibrated age (Cal yBP) 2 σ	Material	Elevation m a.s.l.
5	PS-25-1	Beta-326738-F	6790 \pm 40	-10.8	7680-7580	6480 \pm 90	7507-7165	<i>Fernandezia</i>	85.0804
1	PS-25-7	Beta-326739-R	7860 \pm 40	-8.0	8320-8030	7550 \pm 90	8508-8050	<i>Nerita</i>	69.7153
1	PS-25-7	Beta-307410-F	4580 \pm 30	-8.4	5440-5090	4270 \pm 80	4965-4522	<i>Succinea</i>	69.7153
Data obtained at Beta Analytic Inc., Miami, Florida									
Elevation computed from dGPS data with correction for daily variation of sea level and local height of the antenna									

396

397

398

399

400

401

402

403

404

405

406

407

408

409

410

411

412

413

414

415

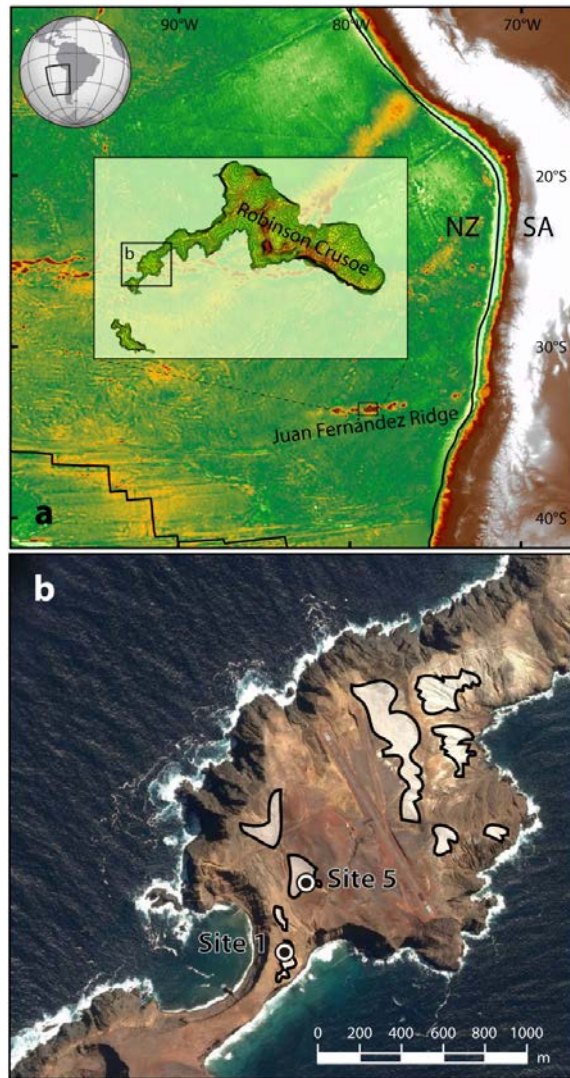
416

417

418

419

420



421

422

423 Figure 1. Location of Juan Fernández Ridge (a), with Robinson Crusoe Island in a box.

424 Below (b) is a satellite image of the southwestern "panhandle" where the aerodrome is

425 situated. White areas are those of the Bahía Tierra Blanca Formation, where a well exposed

426 supratidal Holocene sequence was dramatically uplifted (see text for details). Sampling

427 sites labeled with numbers (see Table 1). NZ: Nazca Plate: SA: South American Plate.

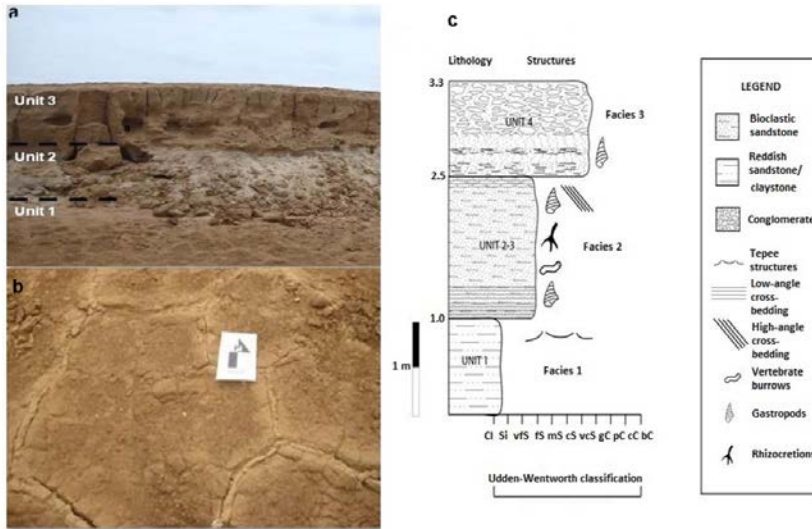
428

429

430

431

432



433

434

435

436

437

438 Figure. 2. Exposure of sedimentary units as described in text (a). *Nerita* dated at *ca.* 8 ka

439 sampled from Unit 1. Below 'teepee' structures in Unit 1 (b), interpreted as part of a former

440 supratidal flat. A composite stratigraphic column (c) from records at sites shown in Figure

441 1.

442

443

444

445



446

447

448

449

450

451 Figure 3. *Nerita* shells found in eolian deposits of Unit 2. These are marine species,
452 probably incorporated into dunes developed close to the supratidal flat shoreline. Visual
453 field is 2.5 cm.

454

455

456